Design of a Miniaturized Split-Ring Resonator Based UWB Notched Bandpass Filter

Piali Chakraborty[1, *], Jyoti R. Panda[1], Arindam Deb[2], Sudhakar Sahu[1], and Jibendu S. Roy[1]

Abstract—A compact selective ultra-wideband (UWB) bandpass filter primarily based on a multi-mode resonator is presented in this paper. A modified elliptical split-ring resonator (SRR) embedded in a variant of the ring resonator is employed to configure a microstrip UWB triple-notched bandpass filter with improved in-band and out-of-band filter properties. Further, the bent inter-digital coupled lines with apertures at the backside are applied to overall filter size miniaturization apart from contributing tight coupling through the entire structure. The three notches facilitated by the modified elliptic SRR have gained the ability to suppress the wireless local area network (WLAN) (5.48 GHz), C band RADAR (7.68 GHz), X band RADAR (8.82 GHz) interfering signals profoundly within the UWB. Simultaneously, the other filter attributes likely a uniform forward transmission coefficient with minimum attenuation (0.46 dB ∼ 1.52 dB), a high skirt factor (0.88), a wide passband (6.52 GHz) with high fractional bandwidth (FBW) (103.16%), broad upper stopband (3.47 GHz), etc. together establish the proposed filter, suitable for practical UWB applications. The uniqueness of this design lies in the flexibility to configure the filter as either a double-notched or a triple-notched bandpass filter by altering only the aspect ratios of elliptical SRR. Simulated filter characteristics are compared with the results obtained by measuring the fabricated prototype, and a good accordance between the compared outcomes validates the design pertinence well.

1. INTRODUCTION

Since 2002, Federal Communications Commission (FCC) has allocated an ultra-wide spectrum range covering frequencies from 3.1 GHz to 10.6 GHz for non-licensed commercial usage [1]. Although this huge band is already shared by some well-known authorized radio sources namely WiMAX (3.5 GHz), WLAN (5 GHz, 5.9 GHz), Wi-Fi (6 GHz), C band (4 GHz ∼ 8 GHz) radar, satellite communication (8 GHz), and X band radar (8 GHz ∼ 12 GHz), etc., the innate characteristics of UWB communication system can insulate its signals from being adulterated with the other radio signals existing in the band. A UWB radio system utilizes an extremely narrow duration (0.1–2 ns) burst of modulated radio frequency (RF) energy for information transmission. So, the emitted spectrum possesses very low (< 1 mw) energy density, shielding the desired signals. However, the UWB spectrum causes congestion with other existing wireless services. To resolve this issue, researchers have introduced notches in the passband centering other source cutoff frequencies. Notches can be achieved by incorporating some additional stubs, different microstrip resonating structures, defected ground structure (DGS), SRR, etc. into the primary design of the UWB filter as reported in the literature [2, 3]. Some recent UWB communication systems with their notch generation techniques having worthwhile contributions in the

frequency shielding process and applicable in both microwave antenna and bandpass filter circuits are reviewed thoroughly and discussed below.

For example, electromagnetic bandgap (EBG) unit cell of Archimedean spiral shape is implemented in both UWB monopole antenna and multi mode resonator (MMR)-based ring stub attached UWB bandpass filter for interfering frequency suppression [4]. Archimedean spiral electromagnetic bandgap (ASEBG) structure is also applied to an existing double-notch UWB bandpass filter comprising a defected L-shaped microstrip structure along with a T-shaped resonator to realize triple-notch bandgap characteristics [5]. Another type of well-known UWB passband development technique is the surface-to-surface transition between the microstrip on the top of the substrate and the short-circuited coplanar waveguide on the ground. Alteration of the shape of coplanar waveguide (CPW) and embedding of differently shaped resonators within the microstrip is used as a notch-generating tool. For example, the engraving of two integrated DGSs namely C-shaped resonant ring (CSRR) and complementary folded split ring resonator (CFSRR) in the CPW led to three notches in the basic UWB passband generated by two microstrip to CPW transition arrangements placed on either side of the substrate [6]. Retaining dimensions of a CPW-fed monopole radiator fixed in the ground plane, a dual notch property can be exhibited by two sets of square SRR on the top plane coupled inductively to the radiator [7]. The method of implementing a combination of slot etched semi-ellipse structure in the ground plane and U-shaped resonators short-circuited with a microstrip line for securing basic UWB filter characteristics and applying quarter wavelength open-circuited stubs loaded to the microstrip line for notch formation can also be noted [8]. Besides, a CPW through line on the top plane possessing broadside coupling with a U-shaped open-ended half wavelength CPW resonator in the ground plane is introduced where a high Q factor is produced by the microwave power flow in the coplanar waveguide through line (CPWTL) which occurs over a narrow region [9]. Next exploiting MMR as an elementary UWB filter designing mechanism and inclusion of various stubs, stepped impedance resonator (SIR), and different novel structures in it is the way to introduce notches at desired frequencies. For instance, methods like loading four stepped impedance open stubs to the uniform transmission line (UTL) by analytical approach, a combination of four quarter-wavelength short-circuited stubs, E-shaped and T-shaped resonators coupled with the transmission line, a comb-shaped resonator, and downward extended inter-digital lines coupled to uniform impedance resonator (UIR) loaded with SIR structures are worth mentioning [10–12]. Using two types of stub-loaded shorted SIRs placed inside and outside the stub loaded ring resonator (SLRR) is a process of the aforementioned kind [13]. Also, a multiple-mode H-shaped ring resonator is used to improve passband selectivity while the half-wavelength and quarter-wavelength resonators are employed to develop in-band rejection characteristics [14]. UWB filter band-stop property can be achieved by the open-circuited stubs (OCSs) amended with a single couple line section, and simultaneously filter selectivity is enhanced by two-unit cells of inline structure connected in parallel to each other [15]. Aside from that, notch generation process by a short stub resonant network loaded with an LC resonator and π resonator is also reported [16]. Two ground plane parasitic resonators of iron shape and inverted U shape symmetric about the feed line and radiating circular patch on the top plane can develop dual notches in the passband [17]. The UWB bandpass filter (BPF) realized by slow wave half mode substrate integrated waveguide (SIW) structure with spiral microstrip resonant cells engraved on it is studied where a quarter-wavelength short-circuited L type resonator is employed to fetch a notch in the passband [18].

Though numerous research works have enriched the literature, a lot of scopes exist in this context in terms of structural novelty, filter size contraction, etc. for becoming utterly applicable in practical uses like imaging systems, radar systems, high-speed home, and business networking devices, etc. In this paper, the authors have presented a new notch-generating structure while simultaneously keeping the filter size small. The filter designing and performance evaluation steps are executed using high-frequency structure simulator (HFSS) V13 software [19]. Arlon material having relative dielectric constant $\varepsilon_r = 2.5$, thickness $t = 0.8\,\text{mm}$, and dielectric loss tangent $\delta = 0.0015$ is used for the fabrication of the filter.

The novel approaches of the proposed design are enlisted in this paragraph as follows: 1) The filter configuration is a combination of MMR, ring, and split-ring resonator, where the SRR is embedded as the integrated part of the ring. 2) A ring resonator of a particular shape and a modified elliptical SRR have been explored jointly as a notch generation technique. 3) This filter can be designed either

as a double-notched band or a triple-notched band filter as per requirement. A different value aspect ratio of the ellipses that have been used to form the elliptical SRR can bring the desired results keeping all other dimensions unchanged. 4) High impedance line sections of the MMR and its adjacent inter-digital coupled lines are molded into a Z shape and inverse Z shape towards the input and output ports, respectively, benefiting substantially in the effective filter size reduction process.

2. STRUCTURAL COMPOSITION AND SIMULATED RESPONSES

2.1. Design of Notched Band UWB Bandpass Filter

The primary UWB bandpass filter is achieved by the conventional MMR method where Z-shaped bent inter-digital coupled lines with L-shaped apertures at the backside are applied to overall filter size miniaturization apart from contributing to tight coupling between individual components throughout the design. Next, the incorporation of notches in the passband by a ring structure accompanied by a modified elliptic split-ring resonator to capacitate the filter as interference-resistant is accomplished. The ring resonator is mounted on the MMR by a vertical stub to fetch a notch at 7.68 GHz. Adding a short-ended line section inside the ring enhances the attenuation level of the created notch. Now a modified elliptical SRR is embedded within the ring through the very horizontal shorted line without occupying any additional area to increase the filter size, contributing two more notches at 5.48 GHz and 8.82 GHz. Here two open-ended stubs suspended from the ports and one short-ended shaft-like stub suspended from the MMR are used for compensating the losses in the input reflection coefficient. The SRR is illustrated separately in Subsection 2.4 for clear perception. In the simulation, a large number of parametric studies by changing different dimensions of the ring resonator are performed to obtain the best characteristics of the filter, and then the final dimensions of the bandpass filter are determined. The final dimensions related to Fig. 1 are denoted below. All dimensions are in mm.

(a)

(b)

(c)
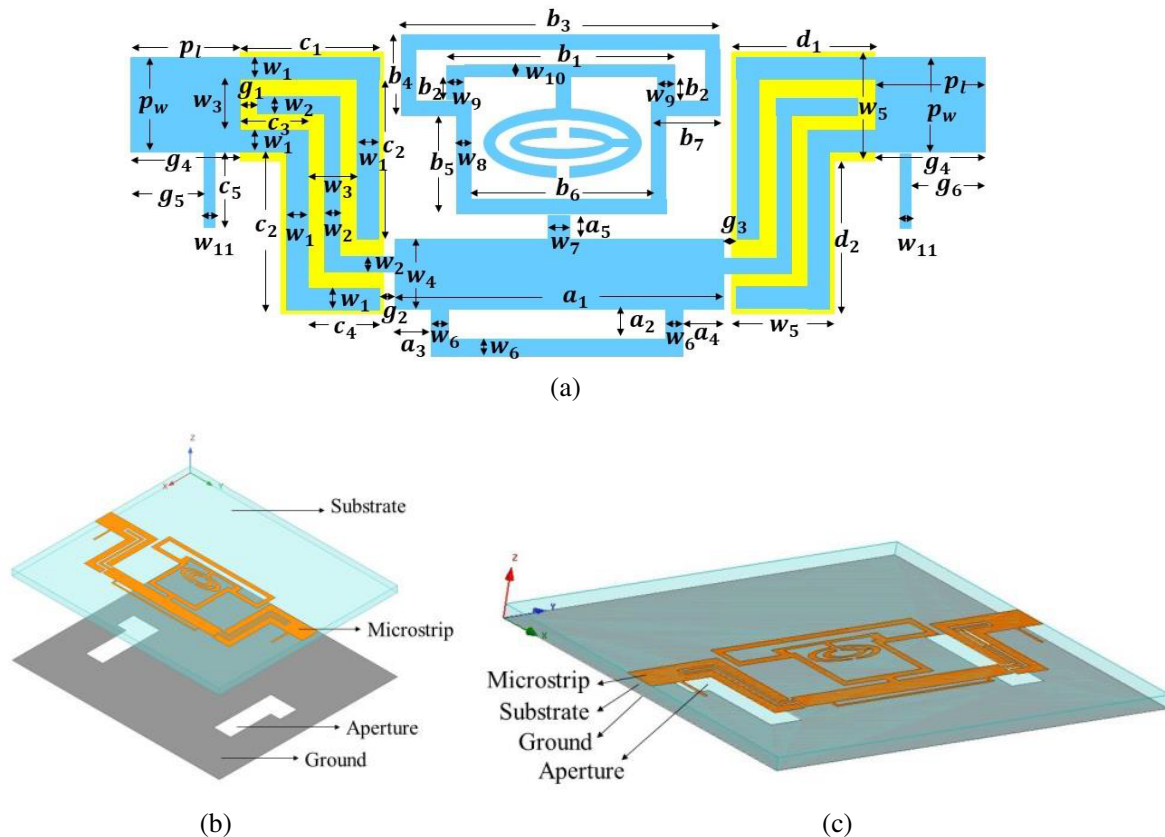
Figure 1. Geometry of the notched band UWB bandpass filter, (a) top view, (b) isometric view, (c) perspective view.

$a_1 = 15$, $a_2 = 0.4$, $a_3 = 1.74$, $a_4 = 1.66$, $a_5 = 0.47$, $b_1 = 7.6$, $b_2 = 0.55$, $b_3 = 14.5$, $b_4 = 2.5$, $b_5 = 4.5$, $b_6 = 5.5$, $b_7 = 4.5$, $c_1 = 3.46$, $c_2 = 5.72$, $c_3 = 2$, $c_4 = 1.46$, $c_5 = 2.25$, $d_1 = 3.56$, $d_2 = 5.5$, $g_1 = 0.21$, $g_2 = 0.2$, $g_3 = 0.18$, $g_4 = 3$, $g_5 = 2$, $g_6 = 1.8$, $p_l = 3$, $p_w = 2.2$, $w_1 = 0.74$, $w_2 = 0.3$, $w_3 = 0.72$, $w_4 = 1.4$, $w_5 = 2.2$, $w_6 = 0.2$, $w_7 = 0.6$, $w_8 = 0.5$, $w_9 = 0.7$, $w_{10} = 0.3$, $w_{11} = 0.2$.

2.2. Chronological Structure Advancement towards Notch Generation

The step-by-step gradual advancement process of the proposed notched band UWB bandpass filter is described explicitly in Fig. 2. Additionally, output characteristics of each step in terms of forward transmission coefficient are illustrated in Fig. 3. The first step is the generation of basic UWB bandpass filter by an inter-digitally coupled MMR structure. Further, the two inverted L-shaped apertures at the backside on the ground plane underneath the inter-digital coupled lines are significantly accounted for establishing a strong coupling between the filter elements and the ports resulting in proper input/output port impedance matching. Output characteristics include a steady 6.67 GHz wide 3 dB passband expanding from 3.03 GHz to 9.7 GHz, average induced insertion loss throughout the passband of 0.47 dB while the maximum insertion loss is 1.34 dB, a highly attenuated (20 dB) broad (2.23 GHz) upper stopband, and 0.25 ns uniform group delay. Two open-ended stubs suspended from the ports are used for compensating the losses in the input reflection coefficient curve in this stage. The ring structure mounted on the MMR in the second stage improves the filter selectivity enormously by adding a lower transmission zero at the lower edge of the passband. Also, a notch is initiated in the passband. Next, in the third stage loading a short-ended line section inside the ring reduces the insertion loss of the induced notch in the previous stage. Moreover, a shaft-like structure is added to the MMR in the fourth stage to enhance the input reflection coefficient curve standard. Finally, in the last stage, a modified elliptical SRR is suspended from the short-ended line section emerging two highly attenuated sharp notches at 5.48 GHz and 8.82 GHz in the passband.

(a)   (b)   (c)

(d)   (e)
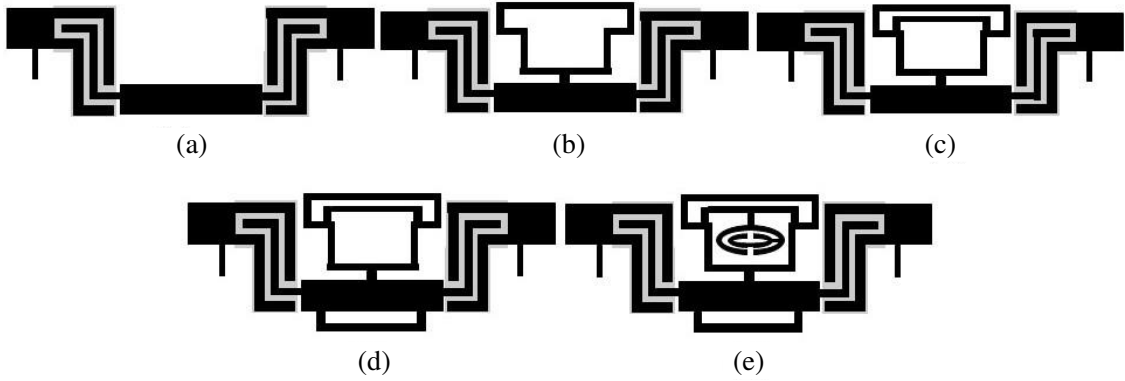
Figure 2. Evolution process of the proposed bandpass filter, (a) stage 1, (b) stage 2, (c) stage 3, (d) stage 4, (e) stage 5.
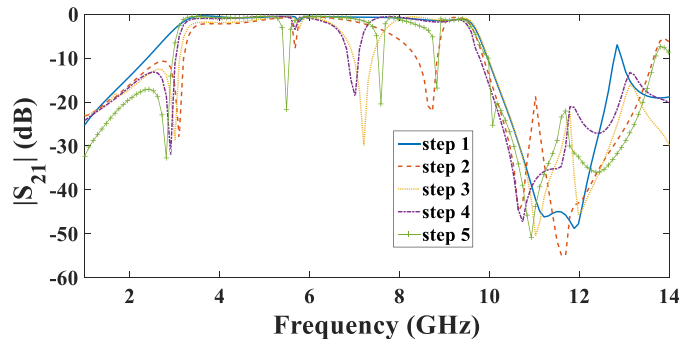
Figure 3. Stepwise $|S_{21}|$ response comparison of respective stages.

2.3. Analysis of Ring Attached MMR Structure

The ring structure associated with MMR is analyzed by separating it into even and odd modes due to its vertical symmetry as presented in Fig. 4. Simulated resonant peaks appear at 3.29 GHz, 4.15 GHz, 6.06 GHz, 7.3 GHz, and 8.92 GHz. Input admittances regarding even mode and odd mode are calculated as $Y_{\text{in, even}}$ and $Y_{\text{in, odd}}$, respectively, while internal input admittances can be determined from the characteristics admittance Y and electrical length θ of each transmission line section which is also computed from the physical dimensions of the lines as mentioned in Fig. 1. The length of the modified ring is $2l$ where $l = b_3/2 + b_4 + b_5 + b_6/2 + b_7$, and the length of the shaft attached with MMR is assumed as $2k$ where $k = (a_1/2 - a_3) + a_2 + w_4$. Equations that express $Y_{\text{in, even}}$ and $Y_{\text{in, odd}}$ are given below [20].

$$Y_{\text{in, even}} = Y_1 \left(Y_{in2} + jY_1 \tan\theta_1 \right) / \left(Y_1 + jY_{in2} \tan\theta_1 \right) \tag{1}$$

where,

$$Y_{in2} = Y_2 \left(Y_{in3} + jY_2 \tan\theta_2 \right) / \left(Y_2 + jY_{in3} \tan\theta_2 \right) \tag{2}$$
$$Y_{in3} = Y_3 \left(Y_{in4} + jY_3 \tan\theta_3 \right) / \left(Y_3 + jY_{in4} \tan\theta_3 \right) \tag{3}$$
$$Y_{in4} = Y_4 \left(Y_{in5} + jY_4 \tan\theta_4 \right) / \left(Y_4 + jY_{in5} \tan\theta_4 \right) \tag{4}$$
$$Y_{in5} = Y_5 \left(Y_{in6} + jY_5 \tan\theta_5 \right) / \left(Y_5 + jY_{in6} \tan\theta_5 \right) \tag{5}$$
$$Y_{in6} = Y_6 \left(Y_{in7} + jY_6 \tan\theta_6 \right) / \left(Y_6 + jY_{in7} \tan\theta_6 \right) \tag{6}$$
$$Y_{in7} = Y_7 \left(Y_{in8} + jY_7 \tan\theta_7 \right) / \left(Y_7 + jY_{in8} \tan\theta_7 \right) \tag{7}$$

and

$$Y_{in8} = -jY_8 \cot\theta_8. \tag{8}$$

Simplification of $Y_{\text{in, odd}}$ includes Equations (1)–(3) where Y_{in4} is interpreted as

$$Y_{\text{in4}} = -jY_4 \cot\theta_4 \tag{9}$$

and $Y_{\text{in, even}}$ is replaced by $Y_{\text{in, odd}}$. Three even mode resonant frequencies such as f_{e1}, f_{e2}, f_{e3}, and two odd mode resonant frequencies namely f_{o1}, f_{o2} achieved by evaluating the aforementioned equations maintain close similarity to simulated resonant peak values thus substantiating the design.

The length, width, and shape of the ring have a crucial effect on the resonant peaks as presented in Fig. 5(a). Below 20.5 mm and above 22.5 mm, the peak f_{e2} disappears. Besides f_{e2} and f_{e3}, it maintains a constant quality only for the optimized ring width of 0.5 mm. Fig. 5(b) describes the influence of the length and width of the stub through which the ring is mounted on the MMR. When the length is considered as greater/smaller than 0.47 mm, f_{e1} and f_{e3} are noticed to diverge accordingly from the expected range. The impact of the shaft-like structure of length k is presented in Fig. 5(c). Considering k, lower than 6.74 mm, it pushes f_{o2} away steadily from the upper edge of the passband. Lastly, in
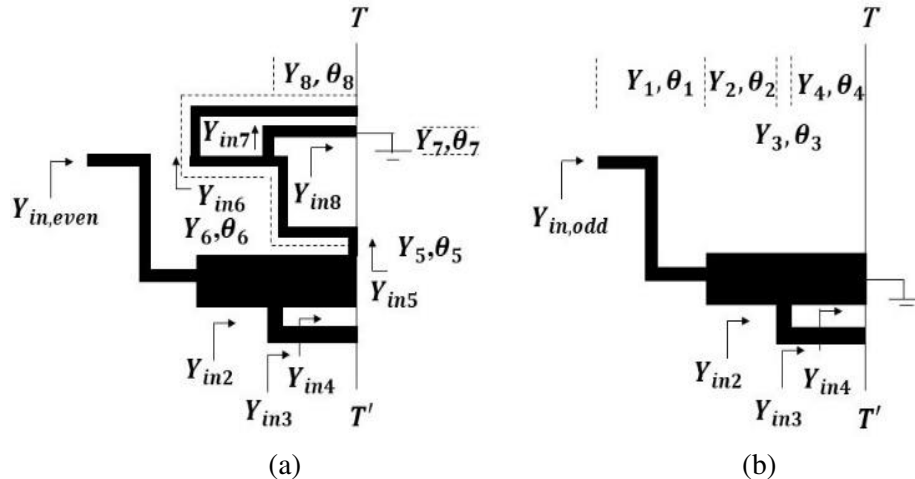
Figure 4. Equivalent circuit of MMR attached ring structure, (a) even mode, (b) odd mode.
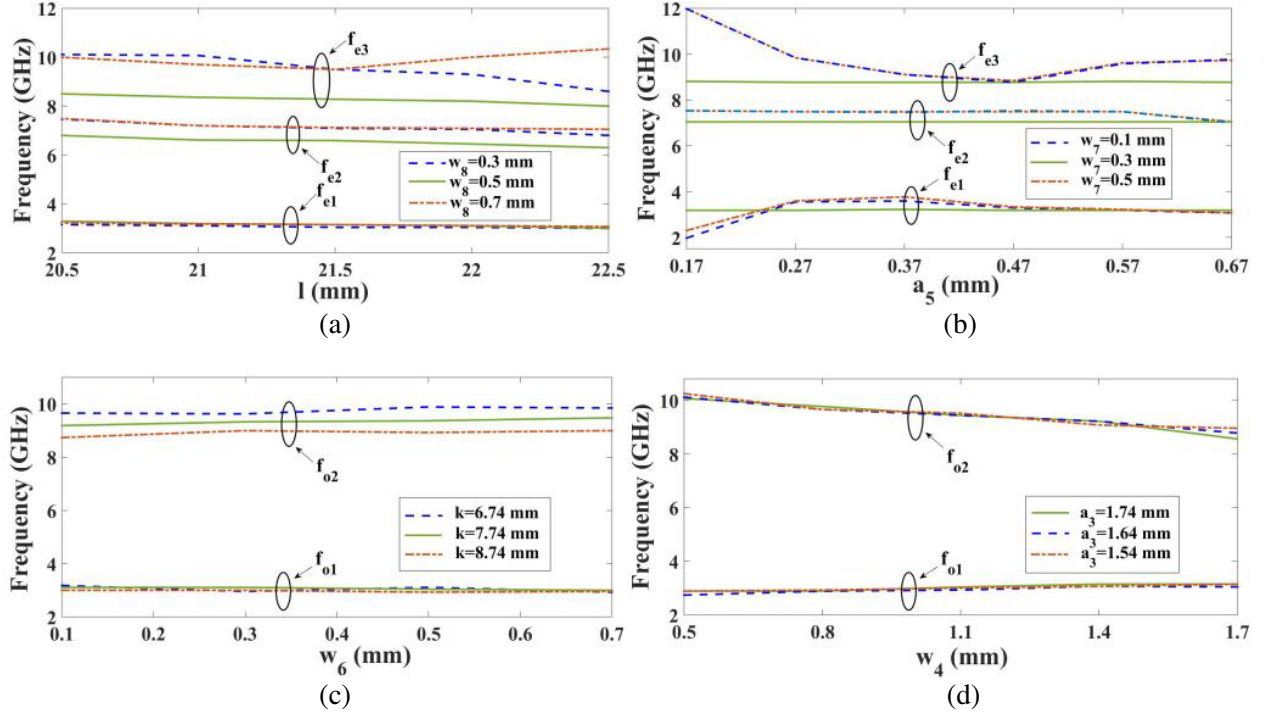
Figure 5. Response of the resonant frequencies under variation in dimensions of the resonators, (a), (b) even mode frequencies, (c), (d) odd mode frequencies.

Fig. 5(d) the odd resonances are marked to be optimized gradually with the increasing width of the MMR. Initially, the first odd resonance occurred at a lower value and the second odd resonance at a higher value than in the simulation process but near the optimized width of 1.4 mm, f_{o1}, f_{o2} match with the simulated values closely.

2.4. Double/Triple Notched Passband Presentation by Elliptical SRR

The modified elliptical SRR produced in this design has acquired an exclusive property to produce a double-notched passband or triple-notched passband while maintaining the remaining output characteristics intact. Fig. 6(a) delineates the modified SRR structure where point o, situated on the central vertical axis TT' is the center of the elliptical resonators. Here twice the distance from point o to x_1, i.e., $2m_{x1}$, indicates the outer major axis of the outer ring. Similarly, $2m_{x2}$ is the inner major axis of the outer ring. On the other hand, for the inner ring, $2m_{x3}$ and $2m_{x4}$ are measured as outer and inner major axes, respectively. The minor axes corresponding to the outer ring and inner ring are $2m_{y1}$, $2m_{y2}$ and $2m_{y3}$, $2m_{y4}$, respectively. The ratio of the major axis value to the minor axis value is defined as the aspect ratio as represented by Equation (10).

$$E_{ari} = \frac{m_{xi}}{m_{yi}} \quad \text{where } i = 1...4 \tag{10}$$

A double-notched passband is achieved by taking all the aspect ratio values of 2.2. Two notches appeared at 5.58 GHz and 8.06 GHz with high attenuation of 22.21 dB and 20.84 dB, respectively. Now, considering $E_{ar1} = 2.5$ and other aspect ratios as 2.45 without varying the major axis lengths a triple-notched one can be achieved. Obtained notch frequencies are 5.48 GHz, 7.58 GHz, and 8.82 GHz with rejection capacity 21.66 dB, 20.47 dB, and 16.77 dB correspondingly. The required optimized dimensions to draw this modified elliptical SRR are measured in mm and mentioned below. E_{ari} values are given in Fig. 6(b).

$e_1 = 0.32$, $e_2 = 0.14$, $e_3 = 0.08$, $e_4 = 0.52$, $e_5 = 0.25$, $e_6 = 0.76$, $e_7 = 0.4$, $m_{x1} = 1$, $m_{x2} = 0.8$, $m_{x3} = 0.6$, $m_{x4} = 0.4$.
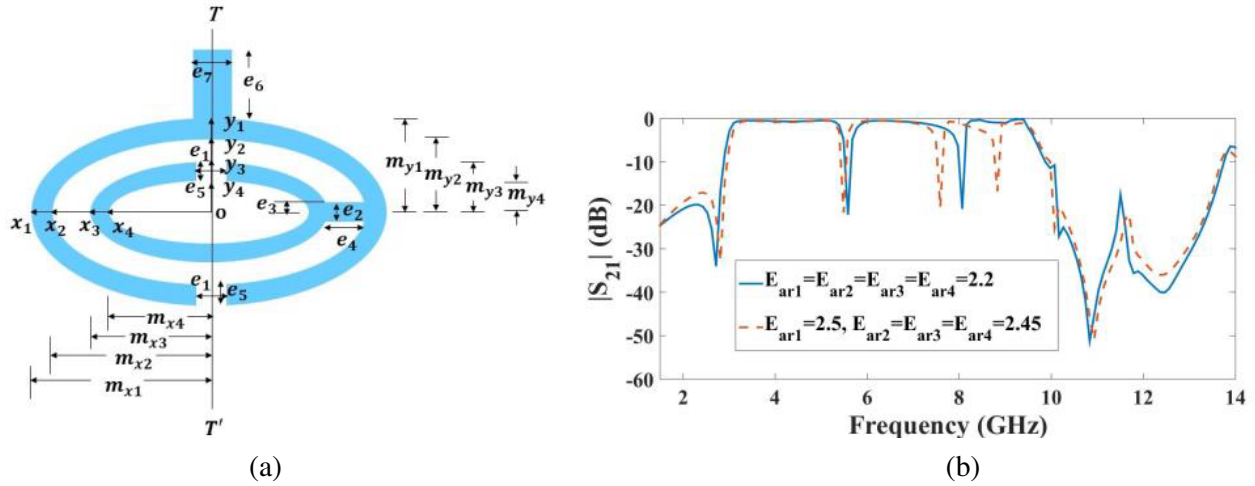
Figure 6. (a) Modified elliptical SRR structure, (b) double/triple notched passband related to different dimensions of the SRR.

2.5. Simulation Results

A parametric analysis of the key notch attributes controlling elements is accomplished and explicated in Fig. 7. The role of the aspect ratio of the elliptic SRRs is encapsulated in Fig. 7(a). This parametric study is conducted by taking all aspect ratios from E_{ar1} to E_{ar4} equal at a time. Ratios can also be varied to obtain an optimized result. At a small ratio of 1.99 double notched band started to form with comparatively lower notch attenuation of 13 dB and raised to a level greater than 20 dB gradually at a ratio of 2.2. The further increment can bring three notches in the passband, and all three notches
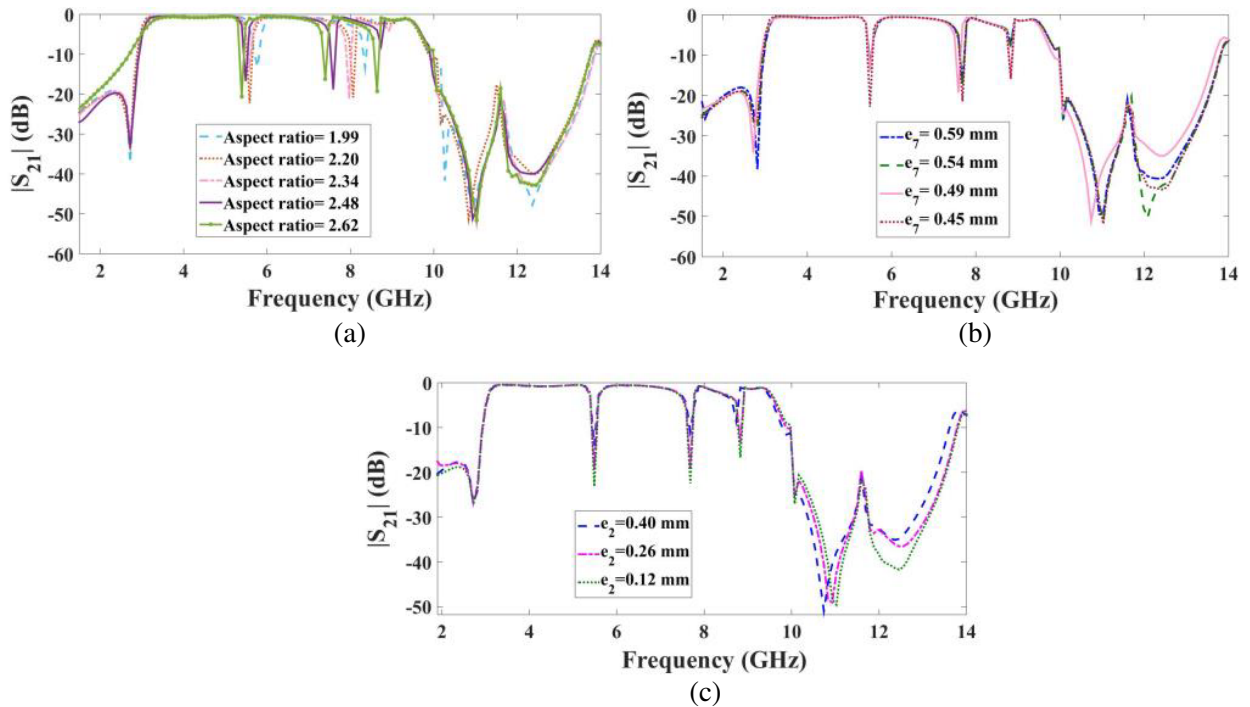
Figure 7. Magnitude of $|S_{21}|$ parameter, (a) for different aspect ratios, (b) for different value of width e_7, (c) for different value of width e_2.

are slightly shifted towards the lower frequency range simultaneously. This way it can be noted that a 2.62 or higher value of aspect ratio can degrade the overall filter response, and like at 2.62 the lower transmission zero disappears impeding the sharp transition of signal from the stopband to the passband.

Fig. 7(b) and Fig. 7(c) respectively discuss the impact of two modifications applied to elliptical SRR namely 1) a vertical stub of width e_7 that joins the SRR with the ring through a short ended line section and 2) a connecting microstrip line between two elliptic split-rings of width e_2. By decreasing e_7 gradually to an optimized value while keeping other parameters fixed, the rejection capability of three generated notches can be enhanced to a great extent. In this context, the notch that appeared at 7.58 GHz, the outcome of the ring and adjoining short-ended lines, varies slightly with the changes in e_7. On the contrary, e_2 holds an immense impact on the overall notch performance of the filter. The suppression capacity of the notches is improved profoundly by optimizing the width e_2. Reducing e_2 gradually from 0.4 mm, steep notches possessing the highest level of rejection are finally acquired at 0.12 mm. Finally, Fig. 10(a) summarizes all the in-band and out-of-band filter characteristics achieved by the proposed design. The triple notched passband is further improved in terms of rejection capability of notches compared to the triple notched passband offered in Fig. 6(b) by setting $e_2 = 0.12$ mm rather than 0.14 mm and $e_3 = 0.07$ mm rather than $e_3 = 0.08$ mm. A 6.52 GHz wide passband contains three sharp notches at frequencies 5.48 GHz, 7.68 GHz, and 8.82 GHz yielding a degree of rejection levels like 23.17 dB, 22.5 dB, and 16.71 dB, respectively. Filter passband expanding over 3.06 GHz to 9.58 GHz is isolated from out-of-band interfering signals by two stopbands at two edges of the passband. The lower stopband is 1.83 GHz wide and attains a suppression level of 17.04 dB while the upper stopband ranges from 10.04 GHz to 13.51 GHz, and is 3.47 GHz wide with high attenuation level of 20.71 dB. Additionally, the occurrence of a lower transmission zero at 2.71 GHz having a high-level attenuation of 27.09 dB facilitates a steep lower passband edge allowing a sharp signal transition between stopband and passband. A high steep factor of 0.88 strongly preserves the bandpass property for the proposed UWB filter. The insertion loss induced in the passband varies between 0.46 dB and 1.52 dB. The loss level in the input reflection coefficient has been maintained as per the FCC-specified standard of 10 dB. The group delay graph of the designed bandpass filter is plotted in Fig. 10(b) indicating uniformity throughout
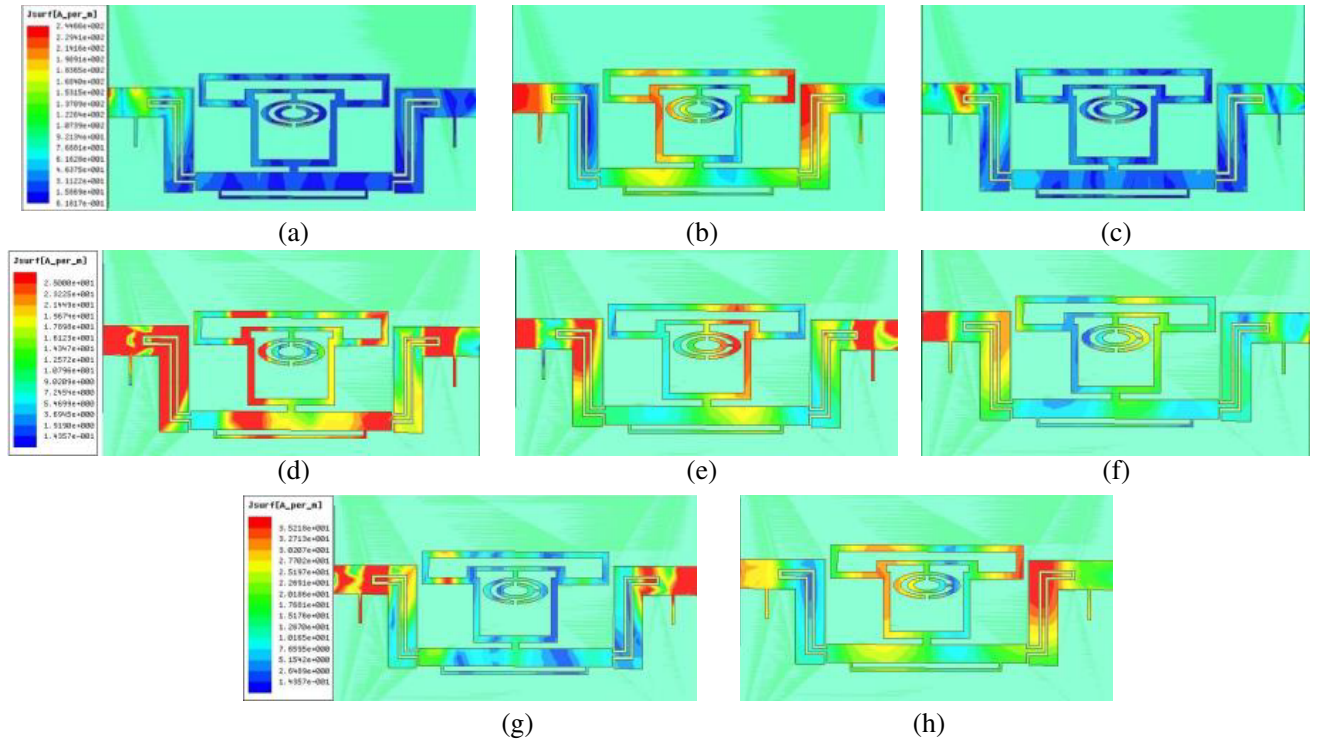
Figure 8. Surface current distribution at (a) 2 GHz, (b) 6.85 GHz, (c) 14 GHz, (d) 5.48 GHz, (e) 7.68 GHz, (f) 8.82 GHz, (g) 3.06 GHz, (h) 9.58 GHz.

the passband with a little variation between 0.29 ns and 0.68 ns except at the notch frequencies.

In the following, a surface current distribution pattern of the filter obtained by simulating the design at different frequencies is produced in Fig. 8. First to infer the workings of the proposed UWB filter, Figs. 8(a), 8(b), and 8(c) are displayed. Next in Figs. 8(d), 8(e), and 8(f), surface current distribution patterns at three notch frequencies such as 5.48 GHz, 7.68 GHz, and 8.82 GHz respectively are illustrated. Finally, the distribution patterns at lower and upper cut-off frequencies are portrayed in Figs. 8(g) and 8(h). The surface current should pass only at the frequencies that exist in the range of the UWB passband (3.1 GHz–10.6 GHz). Three different frequencies such as 2 GHz, 6.85 GHz, and 14 GHz are selected in such a fashion that one is lower than 3.1 GHz (2 GHz), another one is the center frequency that is 6.85 GHz, and the last one is greater than 10.6 GHz (14 GHz). It is observed that surface current is able to move fluently across the filter while operating at 6.85 GHz, but it is noticed to be accumulated in the input port at the frequencies outside the UWB justifying the inherent bandpass feature of the UWB filter. On the other hand, from the large current densities on the ring resonator and elliptical SRR, their active role in obtaining notch behavior can be deduced. Simultaneously at lower (3.06) and upper (9.58) cut-off frequencies input/output ports and interdigital coupled lines hold noticeable surface current density.

A comparative summary of filter output characteristics is reported in Table 1, where the competitiveness of the proposed design can be deduced. The comparison is done with the published papers [6, 10, 11–13, 16, 21, 22].

Table 1. Comparison of the proposed UWB bandpass filter with the published UWB filters.

Published Papers	Filter Structure	ε_r/t (mm)	IL (dB)	USB (GHz)/ Attenuation (dB)	No of notches	Notch frequency (GHz)/ attenuation (dB)	Size $(\lambda_g \times \lambda_g)$
Ref. [6]	DGS with complementary SRR and complementary folded SRR.	10.8/0.635	1.1–1.4	> 5/20	3	5.6, 6.42, 8.03 > 19	1.09 × 0.69
Ref. [10]	UIR loaded with 4 SIRs.	2.2/1.6	< 1.5	> 4.5/20	3	5.18 > 16, 5.86 > 16, 7.92 > 16	1.06 × 0.79
Ref. [11]	Inverted T and E resonator coupled to the transmission line.	3.66/0.762	0.4	N. A	3	3.3/28, 5.1/19, 8.3/15	1.48 × 0.52
Ref. [12]	Comb resonator coupled to SIR loaded UIR.	2.5/0.8	0.3–0.97	5.37/20	3	6/16.16, 6.53/26.27, 8.35/15.22	0.81 × 0.71
Ref. [13]	Stub-loaded ring resonator and shorted stub-loaded SIR.	3.48/0.5	1.3	20/20	3	2.87/33, 5.69/16, 6.5/13	1.44 × 0.49
Ref. [16]	Suspended strip line with LC and π resonator.	3.55/0.254	< 1.3	3.54/27	1	5.82/19	0.73 × 0.34
Ref. [21]	Asymmetric trisection SIR.	2.2/0.787	< 1	12/10	1	5/> 40	0.67 × 0.46
Ref. [22]	Stub loaded SIR.	2.2/0.787	1	1/15.5	1	5.5/> 17	0.67 × 0.39
This paper	Modified elliptic SRR embedded in a ring.	2.5/0.8	0.46–1.52	3.47/> 20.71	3	5.48/23.17, 7.68/22.5, 8.82/16.71	1.02 × 0.34

3. FABRICATION AND MEASUREMENT

To verify the compatibility to be used in UWB devices the proposed filter is fabricated first on the same material which is applied in the simulation process and measured afterward using a vector network analyzer. The obtained S parameters and group delay plots by measuring the fabricated prototype are compared with the simulated outcomes as shown in Fig. 9 and Fig. 10 producing a satisfactory agreement between the results, though slight deviations in measured results for return loss and lower stopband rejection level are noticed. Namely, the measured return loss is 0.59 dB more at 4.3 GHz and 7 dB more at 3.4 GHz than the simulated one. Similarly measured lower stopband rejection level is also 2 dB less than the simulated result. Because of the unpredicted tolerances during the fabrication process and reflections from the SMA connectors measured result slightly deviated from the simulated outcome.

| (a) | (b) |

Figure 9. Fabricated notched band UWB filter, (a) top view, (b) bottom view.

| (a) | (b) |
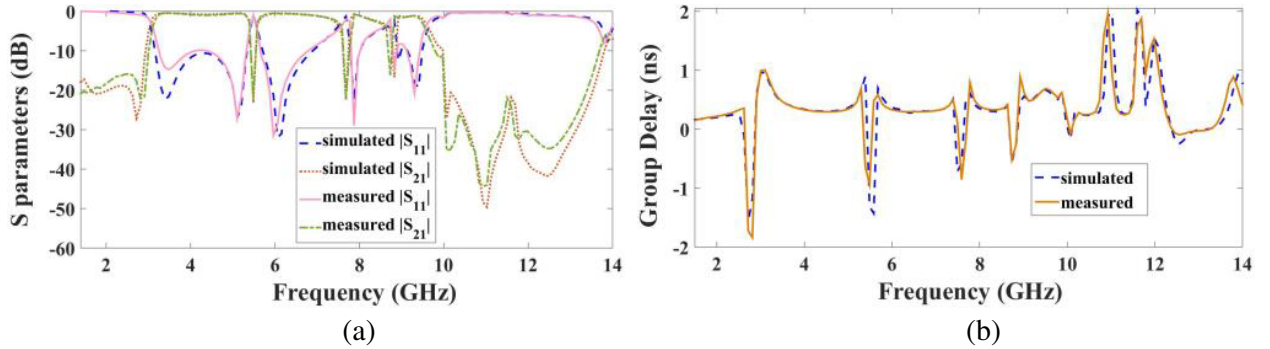
Figure 10. Comparison between simulated and measured outputs, (a) S parameter plots, (b) group delay plots.

4. CONCLUSION

This article develops a UWB bandpass filter where double notched band suppressing WLAN and satellite communication signals, or triple-notched band restraining WLAN, C band, and X band radar interference signals can be obtained by the specified aspect ratio values of modified elliptical split-ring resonators. Emerging notches in the double notched band possess narrow FWBs of 5.54% and 4.76% while for the finally produced optimized triple notched band, 3 dB FWB values of notches are 3.82%, 4.06%, 3.54% having nearly 20 dB high attenuation capacity which ensures a strong obstruction for other radio sources sharing the UWB. Owing to the bent inter-digital coupled line and the distinctive ring shape, the transformation from a basic UWB bandpass filter to a notched band bandpass filter consumes a very small additional effective area, awarding a miniaturized filter size of $1.02\lambda_g \times 0.34\lambda_g$. Simultaneously the other filter attributes likely a uniform forward transmission coefficient with minimum

attenuation ($0.46\,\mathrm{dB} \sim 1.52\,\mathrm{dB}$), a high skirt factor (0.88), a widespread passband ($6.52\,\mathrm{GHz}$) with high FBW (103.16%), broad upper stopband ($3.47\,\mathrm{GHz}$), etc. combinedly establishes the proposed filter suitable for practical applications in UWB devices.

REFERENCES

1. Federal Communications Commission, "Revision of Part 15 of the commission's rules regarding ultra-wideband transmission systems," First Report and Order, FCC 02, V48, Apr. 2002.

2. Hao, Z. and J. Hong, "Ultra wideband filter technologies," *IEEE Microwave Magazine*, Vol. 11, No. 4, 56–68, 2010.

3. Singhal, P. K., S. Mathur, and R. N. Baral, "Ultra-wide microstrip bandpass filter using short circuited stubs," *J. Electr. Electron. Eng. Res.*, Vol. 3, No. 6, 101–10, Aug. 2011.

4. Modak, S., P. P. Shome, Md. A. Halimi, T. Khan, A. A. Kishk, and T. A. Denidni, "Band-stop filtering for electromagnetic interference rejection in printed UWB components using single compact archimedean spiral EBG cell," *Progress In Electromagnetics Research C*, Vol. 126, 23–37, 2022.

5. Zheng, X. and T. Jiang, "Triple notches bandstop microstrip filter based on archimedean spiral electromagnetic bandgap structure," *Electronics*, Vol. 8, No. 9, 964, 1–15, Aug. 2019.

6. Sazid, M. and N. S. Raghava, "Planar UWB-bandpass filter with multiple passband transmission zeros," *AEU-International Journal of Electronics and Communications*, Vol. 134, 1–7, Mar. 2021.

7. Siddiqui, J. Y., C. Saha, and Y. M. M. Antar, "Compact dual-SRR-loaded UWB monopole antenna with dual frequency and wideband notch characteristics," *IEEE Antennas Wireless Propag. Lett.*, Vol. 14, 100–103, 2015.

8. El Omari El Bakali, H., H. Elftouh, A. Farkhsi, A. Zakriti, and M. El Ouahabi, "Design of a super compact UWB filter based on hybrid technique with a notch band using open circuited stubs," *Advanced Electromagnetics*, Vol. 9, No. 3, 39–46, Dec. 2020.

9. Fahmy, W. M., A. E. Farahat, K. F. A. Hussein, and A.-E.-H. A. Ammar, "High Q-factor bandstop filter based on CPW resonator broadside-coupled to CPW through-line," *Progress In Electromagnetics Research B*, Vol. 86, 121–138, 2020.

10. Taibi, A., M. Trabelsi, and A. A. Saadi, "Efficient design approach of triple notched UWB filter," *AEU-International Journal of Electronics and Communications*, Vol. 131, 1–7, Mar. 2021.

11. Basit, A., M. I. Khattak, and M. Alhassan, "Design and analysis of a microstrip planar UWB bandpass filter with triple notch bands for WiMAX, WLAN, and X-band satellite communication systems," *Progress In Electromagnetics Research M*, Vol. 93, 155–164, 2020.

12. Chakraborty, P., P. P. Shome, J. R. Panda, and A. Deb, "Highly selective UWB bandpass filter with multi-notch characteristics using comb shaped resonator," *Progress In Electromagnetics Research M*, Vol. 108, 89–101, 2022.

13. Wang, C., X. Xi, Y. Zhao, and X. Shi, "Compact tri-notched wideband bandpass filter based on multiple resonances with wide upper stopband," *Microw. Opt. Technol. Lett.*, Vol. 62, No. 12, 3842–3847, Aug. 2020.

14. Gao, Z., P. Wu, and Y. Zhang, "A new compact microstrip ultra-wideband (UWB) bandstop filter with good performance," *Progress In Electromagnetics Research Letters*, Vol. 93, 9–12, 2020.

15. Dardeer, O. M., H. A. Elsadek, H. M. Elhennawy, and E. A. Abdallah, "Ultra-wideband bandstop filter with multi transmission zeros using in-line coupled lines for 4G/5G mobile applications," *AEU-International Journal of Electronics and Communications*, Vol. 131, 1–6, 2021.

16. Xu, Z., "UWB bandpass SSL filter with an adjustable notched band and four transmission zeros," *Electron. Lett.*, Vol. 57, No. 24, 930–932, Nov. 2021.

17. Yadav, D., M. P. Abegaonkar, S. K. Koul, V. Tiwari, and D. Bhatnagar, "A compact dual band-notched UWB circular monopole antenna with parasitic resonators," *AEU-International Journal of Electronics and Communications*, Vol. 84, 313–320, 2018.

18. Li, J., C. Ding, F. Wei, and X. W. Shi, "Compact UWB BPF with notch band based on SW-HMSIW," *Electron. Lett.*, Vol. 51, No. 17, 1338–1339, Aug. 2015.

19. Ansoft Corporation, Ansoft HFSS (Version 13).

20. Zhu, L., S. Sun, and R. Li, *Microwave Bandpass Filters for Wideband Communications*, Ch. 2, John Wiley & Sons, Inc., Hoboken, NJ, 2012.

21. Kumari, P., P. Sarkar, and R. Ghatak, "A multi-stub loaded compact UWB BPF with a broad notch band and extended stopband characteristics," *Int. J. RF Microw. Comput.-Aided Eng.*, Vol. 30, No. 4, 1–8, Jan. 2020.

22. Weng, M. H., F. Z. Zheng, H. Z. Lai, and S. K. Liu, "Compact ultra-wideband bandpass filters achieved by using a stub-loaded stepped impedance," *Electronics*, Vol. 9, No. 2, 1–12, Jan. 2020.